Double-Layer Gadolinium Zirconate/Yttria-Stabilized Zirconia Thermal Barrier Coatings Deposited by the Solution Precursor Plasma Spray Process

Chen Jiang, Eric H. Jordan, Alan B. Harris, Maurice Gell, and Jeffrey Roth

(Submitted April 13, 2015; in revised form July 2, 2015)

Advanced thermal barrier coatings (TBCs) with lower thermal conductivity, increased resistance to calcium-magnesium-aluminosilicate (CMAS), and improved high-temperature capability, compared to traditional yttria-stabilized zirconia (YSZ) TBCs, are essential to higher efficiency in next generation gas turbine engines. Double-layer rare-earth zirconate/YSZ TBCs are a promising solution. From a processing perspective, solution precursor plasma spray (SPPS) process with its unique and beneficial microstructural features can be an effective approach to obtaining the double-layer microstructure. Previously durable low-thermal-conductivity YSZ TBCs with optimized layered porosity, called the inter-pass boundaries (IPBs) were produced using the SPPS process. In this study, an SPPS gadolinium zirconate (GZO) protective surface layer was successfully added. These SPPS double-layer TBCs not only retained good cyclic durability and low thermal conductivity, but also demonstrated favorable phase stability and increased surface temperature capabilities. The CMAS resistance was evaluated with both accumulative and single applications of simulated CMAS in isothermal furnaces. The double-layer YSZ/GZO exhibited dramatic improvement in the single application, but not in the continuous one. In addition, to explore their potential application in integrated gasification combined cycle environments, double-layer TBCs were tested under high-temperature humidity and encouraging performance was recorded.

Keywords	CMAS resistance, double layer, gadolinium zirconate, solution precursor plasma spray, thermal barrier coatings, thermal cyclic durability

Abbreviations

APS	Air plasma spray
CMAS	Calcium-magnesium-aluminosilicate
DSC-TGA	Differential scanning calorimetry-thermogravimetric analysis
DI	Deionized
EDS	Energy dispersive x-ray spectroscopy
GZO	Gadolinium zirconium oxide/gadolinium zirconate
IGCC	Integrated gasification combined cycle
IPB	Inter-pass boundary
LFA	Laser-flash analysis
LPPS	Low pressure plasma spray
OEM	Original equipment manufacturer
PSL	Protective surface layer
SEM	Scanning electron microscopy
SPPS	Solution precursor plasma spray
TBC	Thermal barrier coatings
TGO	Thermally grown oxide
UConn	University of Connecticut
XRD	X-ray diffraction
YSZ	Yttria-stabilized zirconia

1. Introduction

Thermal barrier coatings (TBCs) made primarily of low-thermal-conductivity refractory oxides are applied routinely to insulate underlying hot-section components from the hot gas stream in advanced gas turbine engines. Depending on composition, porosity, and thickness, TBCs can provide up to a 300 °C temperature reduction (Ref 1, 2). 6-8 wt.% yttria partially stabilized zirconia (t'-YSZ) has been the topcoat oxide of choice due to its comparatively high thermal expansion coefficient, high fracture toughness, and low thermal conductivity. However, in order to attain increased engine efficiency, higher engine operating temperatures are necessary (Ref 3, 4). The current maxi-

mum use temperature for YSZ TBCs is limited to about 1200 °C (Ref 5) because of (i) the accelerated transformation from the tetragonal prime to the tetragonal phase,

Chen Jiang, Alan B. Harris and **Maurice Gell**, Department of Materials Science and Engineering, University of Connecticut, Storrs, CT; **Eric H. Jordan**, Department of Mechanical Engineering, University of Connecticut, Storrs, CT; and **Jeffrey Roth**, Institute of Materials Science, University of Connecticut, Storrs, CT. Contact e-mail: chenjiang.chn@gmail.com.

and subsequently to the destructive monoclinic phase, (ii) the sintering-induced loss of strain tolerance, and (iii) the reaction between the YSZ TBC and molten calcium-magnesium-aluminosilicate (CMAS). Under the hotter engine environments, the previously inert ingested airborne particulates begin to stick to TBC surfaces and form low temperature eutectics that penetrate and dissolve TBCs, causing premature failures (Ref 6, 7).

To find a material system that is more compatible with hotter engines, alternative TBC compositions have been explored and studied (Ref 5, 8, 9), including fluorites and pyrochlores (Ref 10, 11), perovskites (Ref 12, 13), garnets (Ref 14, 15) and aluminates (Ref 16). Gadolinium zirconate (GZO) has exhibited desirable properties, such as high melting point ($>2000\ °C$ (Ref 17)], good phase stability (pyrochlore stable up to $1550\ °C$ (Ref 18)], lower thermal conductivity than YSZ (Ref 19) and excellent CMAS resistance (Ref 20). The dissolution of rare-earth zirconates upon contact with CMAS and the formation of a highly stable apatite silicate of $Ca_2RE_8(SiO_4)_6O_2$ were shown effective in blocking further CMAS infiltration, thereby protecting the underlying material (Ref 18, 20, 21).

Despite these attractive properties, GZO has lower fracture toughness than YSZ (Ref 22), which could lead to poor thermal cyclic durability (Ref 23) and compromised erosion resistance (Ref 24). In addition, Leckie et al. found that GZO is not thermodynamically compatible with the Al_2O_3 in the thermally grown oxide (TGO) layer (Ref 25) by forming a porous layer of $GdAlO_3$ that reduces TGO oxidation resistance. Therefore, to better incorporate all the advantages of GZO, the idea of introducing a double-layer TBC system using an YSZ inner layer has been proposed (Ref 26). With a high melting point, good phase stability, low thermal conductivity and excellent CMAS resistance, GZO would function ideally as a protective surface layer (PSL), and the traditional YSZ would perform as an interlayer that ensures a reliable topcoat-TGO adhesion and simultaneously economizes the use of expensive rare-earth elements. In fact such double-layer coatings have been fabricated by EB-PVD and seen substantial service in current generation aviation gas turbines (Ref 10, 18, 20). Air plasma spray (APS) process was also adopted to prepare the double-layer TBCs (Ref 23); in a recent study, coating porosity and GZO stoichiometry were found sensitive to APS processing parameters, and early failure and spallation at the GZO/YSZ interface was observed in dense coatings under the burner rig test (Ref 17). The solution precursor plasma spray (SPPS) process, with the microstructural advantages of stress-relieving through-thickness vertical cracks, ultrafine splats (Ref 27, 28) and easy stoichiometry control, can be a promising alternative to producing GZO/YSZ double-layer TBCs.

Previously, durable SPPS YSZ TBCs with an approximately 50% reduction in thermal conductivity was reported at UConn, by optimizing the unique thermal-conductivity-reducing layered porosity, called inter-pass boundaries (IPBs), inherent to the SPPS process (Ref 29). In this study, a GZO PSL was deposited by the SPPS process on the low-thermal-conductivity YSZ TBCs, creating a GZO/YSZ double-layer structure, with the objective of enhancing coatings' CMAS resistance and high-temperature capabilities while retaining the 50% reduction in thermal conductivity and not compromising other engine-critical properties, such as phase stability and thermal cyclic durability. Effort was spent on developing plasma spray process parameters for the successful deposition of this new material, in order to achieve the desired density, microstructure and excellent bonding at the GZO/YSZ interface. To evaluate the efficacy of the addition of GZO PSLs, a set of CMAS-TBC interaction tests were proposed and performed in comparison with APS YSZ baseline samples. To test the double-layer coatings' potential application in the integrated gasification combined cycle (IGCC) environments, a high-temperature steam rig was also constructed and used to characterize the stability of the ceramic topcoat under a high-temperature humid environment.

2. Experimental Procedures

2.1 Preparation and Characterization of Precursor Solutions

Precursor solutions for the SPPS process use a range of organic and inorganic solutes and solvents (Ref 30–32). To deposit the low-thermal-conductivity YSZ interlayer, precursor solutions were prepared from yttrium nitrate and zirconium acetate (Ref 29). After the exploration of several alternatives, the deposition of GZO PSLs was accomplished by mixing 2.4 moles gadolinium nitrate hydrate (Alfa Aesar, Ward Hill MA) in 1 L zirconium acetate solution (22.8 wt.% ZrO_2 in diluted acetic acid, MEL Chemicals Inc., Flemington NJ). The thermal characteristics, viscosity, and surface tension of precursor solutions affect the interaction with the plasma plume as well as the properties of the deposited coatings (Ref 33). Therefore, they were measured, respectively, with DSC-TGA (10 °C/min with a 100 mL/min N_2 flow, SDT Q-600, TA Instruments, New Castle DE) (Ref 29), Ubbelohde glass viscometers (Cannon Instrument Company, State College PA) in a controlled water bath, and a pendant drop tensiometer (OCA 20, Future Digital Scientific Corp, Garden City NY).

The 1 wt.% aqueous CMAS precursors for the CMAS-TBC interaction tests were prepared by mixing appropriate amounts of salts in deionized water. In order to obtain stable precursors, chelating agents, e.g., ethylenediaminetetraacetic acid (EDTA), were added accordingly, and pH was monitored throughout the process.

2.2 Substrates

All substrates in this study were 25.4 mm in diameter and 3 mm thick. 304/304L stainless steel and graphite disks (Ted Pella Inc., Redding CA) were used for the SPPS process optimization and thermal conductivity measurements, while bond-coated, single-crystal substrates and APS YSZ baseline specimens provided by

Table 1 A summary of all test samples used in this study

Topcoat	Topcoat thickness	Substrates	Tests
SPPS GZO	~150 μm	Graphite planchets	Thermal conductivity measurements
SPPS YSZ	~300 μm	Single-crystal superalloy with LPPS MCrAlY bondcoats	Thermal cyclic durability test, CMAS resistance tests
SPPS GZO/YSZ	~300 μm (~200 μm for YSZ, ~100 μm for GZO)	Grit-blasted 304/304L stainless steel	Process optimization
		Single-crystal superalloy with LPPS MCrAlY bondcoats	Thermal cyclic durability test, CMAS resistance tests
		PWA 1484 with 125 μm APS NiCo-CrAlY bondcoats (Sulzer® AMDRY® 365-2)	High-temperature steam test
APS YSZ	~250 μm	Single-crystal superalloy with LPPS MCrAlY bondcoats	Thermal cyclic durability test, CMAS resistance tests
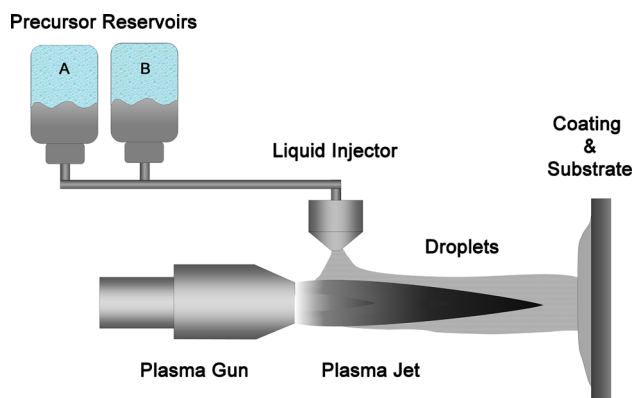
Fig. 1 Schematic illustration of the SPPS process

industrial partners were reserved for critical furnace tests. Limited by the available amount of OEM substrates though, LPPS MCrAlY bondcoats were only used for the thermal cycling and CMAS-TBC interaction tests, while in-house deposited APS NiCoCrAlY bondcoats were utilized for the high-temperature steam test instead, given the sole interest of this test concerned only the ceramic topcoat. The surface roughness of both OEM and in-house fabricated bondcoats were measured to be 4.57 ± 0.29 and 6.26 ± 1.05 μm, respectively. All substrate information is summarized in Table 1.

2.3 TBC Deposition Using the SPPS Process

Both YSZ and GZO layers were deposited using the direct current Metco 9 MB spray system with a 3 MB gas-handling panel (Sulzer Metco, Westbury NY). Specific to the SPPS process (Fig. 1), a customized liquid delivery system was utilized, which included multiple pressurized tanks and an atomizing nozzle. Other details, such as substrates preparation prior to deposition, were discussed elsewhere (Ref 29). Table 2 summarizes the deposition parameters selected for this study.

2.4 Thermal Conductivity of As-Sprayed Coatings

The thermal conductivity of as-sprayed low-thermal-conductivity SPPS YSZ interlayer was measured previously with the laser-flash method (Netzsch LFA 447,

Burlington MA) (Ref 29). The same measurements were performed on the GZO PSLs, in which free-standing specimens were used to minimize the calculation error associated with having multiple layers. Necessary specific heat data were measured with modulated-DSC (TA-Q100, TA Instruments, New Castle DE).

2.5 Microstructural Characterization

Sectioned TBC samples were embedded in a low-viscosity epoxy resin (Allied High Tech Products Inc., Rancho Dominguez CA) for metallography. Field emission scanning electron microscopes (JSM-6350/5F, JEOL USA, Peabody MA) and energy dispersive x-ray spectrometer (Noran system six EDS, Thermo, Waltham MA) were employed for the cross-sectional microstructure characterization; sputtered Au/Pd coatings were frequently applied using a Polaron E5100 SEM Coating Unit.

2.6 X-ray Diffraction

To capture the phase evolution in the SPPS GZO PSLs, TBC samples were periodically scanned by a powder diffractometer (D2 Phaser, Bruker AXS, Madison, WI).

2.7 Thermal Cyclic Durability Test

The cyclic durability performance of the TBC systems on superalloy substrates (Table 1) were compared using 1-h cycles, consisting of 5-min heat-up, 45-min soaking at 1121 °C and 10-min air-forced cooling in a programmable bottom-loading isothermal furnace (CM Furnaces Inc., Bloomfield, NJ), as described in (Ref 29, 34, 35). Multiple TBC samples (four double-layer and two SPPS IPB) were thermally cycled simultaneously. Sample failure was defined as more than 50% area spallation, and then SEM was used to determine spallation sites and TGO thickness.

2.8 CMAS Resistance: Spritz and Paste Tests

Advanced testing designs, e.g., the jet engine thermal shock test (Ref 7, 36) and burner rig tests (Ref 37), are typically employed to evaluate CMAS-TBC interactions under thermal gradient conditions. In this study, a series of relatively simple tests were developed to assess the

Table 2 SPPS process conditions for spraying the GZO PSL and the YSZ interlayer

Parameters	GZO PSL	YSZ interlayer (Ref 29)
Gun power	40-50 kW	45.5 kW
Primary gas/secondary gas	Ar/H$_2$	Ar/H$_2$
Liquid injection mode	Atomization using BETE® spray nozzles	Atomization using BETE® spray nozzles
Liquid flow rates	15-20 mL/min	45-50 mL/min
Standoff distances	38-45 mm	41-47 mm
Traverse speed	450 mm/s	800 mm/s
Cooling time	None	1 min/5 passes
Number of deposition passes	15	30

Table 3 CMAS compositions and melting points

Constituents	Si	Ca	Al	Mg	Na	K	Fe	Ti	S	Melt points
4-CMAS (at.%)	49.47	37.65	7.88	5.00						~1200 °C (Ref 21)
7-CMAS (at.%)	46.34	35.22	7.42	5.47	1.85	1.85	1.85			1132 °C (Fig. 8)
9-CMAS(a)	1.00	0.64	0.61	0.13	0.08	0.06	0.04	0.03	0.59	1180 °C (Fig. 8)

(a) This proprietary composition is normalized at OEM's request
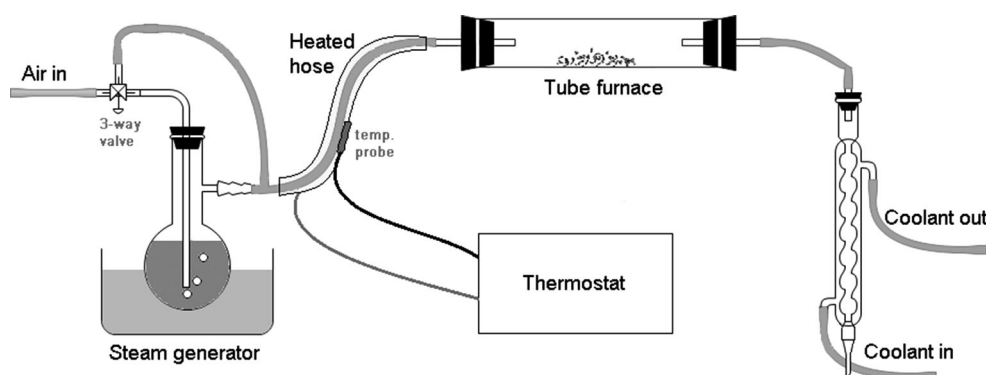
Fig. 2 High-temperature steam test rig

CMAS-TBC interactions and relative improvement of CMAS resistance for the GZO PSL. Different simulated CMAS compositions were used in this study (4-, 7- and 9-CMAS as listed in Table 3, each named after the number of nominal constituents in the thermally decomposed mixes). The melting points of the compositions 7-CMAS and 9-CMAS were measured by DSC-TGA.

To simulate the periodic uptake of traceable amounts of CMAS during engine operation, samples were isothermally cycled to 1180 °C using 1 h cycles. During the cooling stage, when the samples were at approximately 400 °C, CMAS precursor solutions were sprayed over the TBC surfaces with medical bottle atomizers (0.1 mL/spray, LMA MADomizer™, San Diego, CA), one spritz every cycle. One SPPS YSZ sample was also sprayed with DI water to determine if thermal shock was a significant source of damage during this experiment. The temperature for applying liquid CMAS precursor involved compromise between applying it at a realistically high temperature and not creating excessive thermal shock from applying water-based liquid. The temperature of 400 °C was chosen as a somewhat arbitrary compromise,

yet the study of this temperature effect was beyond the scope of the current project.

For more severe testing conditions, samples were also spread with a CMAS paste (25 wt.% 7-CMAS paste, other ingredients including deionized water and a low-viscosity Allied High-Tech epoxy resin) prior to the cyclic durability test. The final dose of the 7-CMAS paste was determined to be 10 mg/cm^2 (equivalent to 25 spritzes of liquid CMAS precursors), based on the reported minimum CMAS level to initiate TBC damage by Wellman et al. (Ref 38). Cycles to failure and spallation mechanism were examined for each TBC system.

2.9 High-Temperature Steam Test

The high-temperature steam corrosion resistance of two double-layer SPPS TBC specimens was evaluated by controlling the humidity within a tube furnace (Fig. 2); testing conditions were chosen from relevant works (Ref 39). The temperature was set to 1121 °C, and the moist air (air + 30% H$_2$O) was disconnected from the quartz tube until the set temperature was reached, so that exact

reaction time was maintained. The hot-zone temperature was confirmed with a K-type thermocouple inserted next to the test piece, in addition to the B-type one resident in the furnace. The testing environment in this setup was reaching the upper application limit for K-type thermocouple; however, the temperature agreement between the K-type and B-type thermocouples was mostly acceptable ($< \pm 5$ °C), suggesting the deterioration of the thermocouple was not a major concern. All samples were heat-

treated for 300 h, and an x-ray diffraction pattern was collected every 50 h.

3. Results and Discussion

3.1 Precursor Characteristics

Generally speaking, precursors with high molarity, manageable viscosity (depending on specific delivery system), predominantly exothermic decomposition reactions, and minimal abrupt release of gases are best suited to the SPPS process. In order to help anticipate and understand the deposition of the GZO PSL, precursor solutions were subject to thermal and rheological characterization that had previously proven to be effective for aiding in depositing YSZ TBCs and magnesia/yttria composites (Ref 33).

Since the primary component of both GZO and YSZ precursor solutions is zirconium acetate, their thermal characteristics are shown to be similar in DSC-TGA tests (Fig. 3): both exhibited predominantly exothermic decomposition reactions above 250 °C. The only major difference between the two precursor solutions is the amounts of nitrates mixed in each solution. The relative concentrations of the oxidizer (nitrate) and the reducer (acetate) in the precursor solution determine the degree of the redox reaction, and maximum exothermic heat is expected when perfect stoichiometry is reached. Both YSZ and GZO precursors are calculated to be predominantly
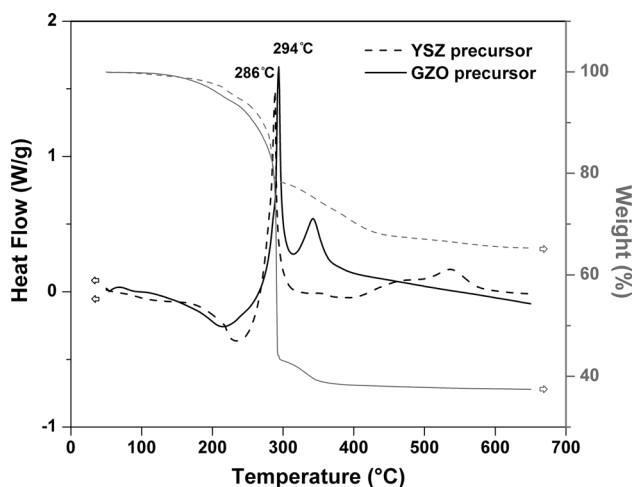

Fig. 3 Thermal characteristics of GZO and YSZ precursor solutions

Table 4 Fluid and thermal properties of GZO and YSZ precursor solutions

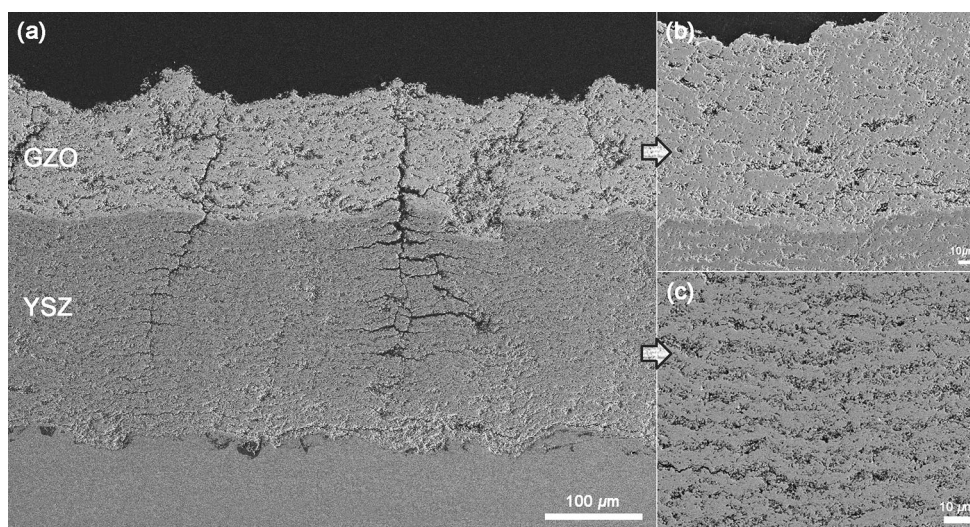| Precursor types	Viscosity, cP	Surface tension, mN/m	Endothermic heat, J/g	Exothermic heat, J/g	Net heat, J/g
GZO, aqueous	6.04	69.37	−121.8	368.7	246.9
YSZ, aqueous	6.16	52.65	−33.4	419.1	385.7

Fig. 4 Typical cross-section micrograph of double-layer SPPS TBC with a GZO protective surface layer (~100 μm) and a YSZ inter-layer with conductivity-reducing IPBs (~200 μm)
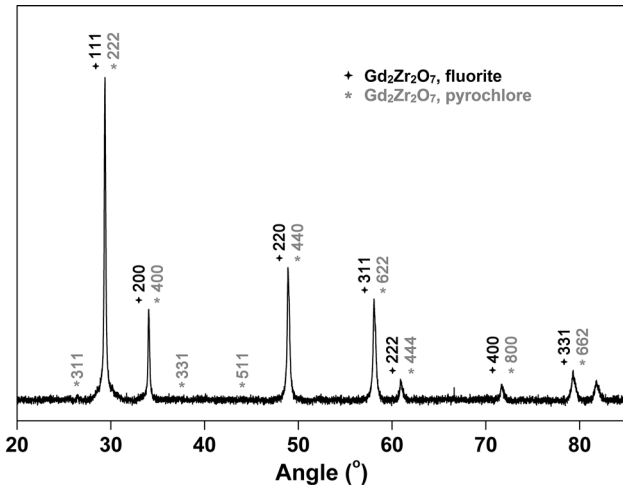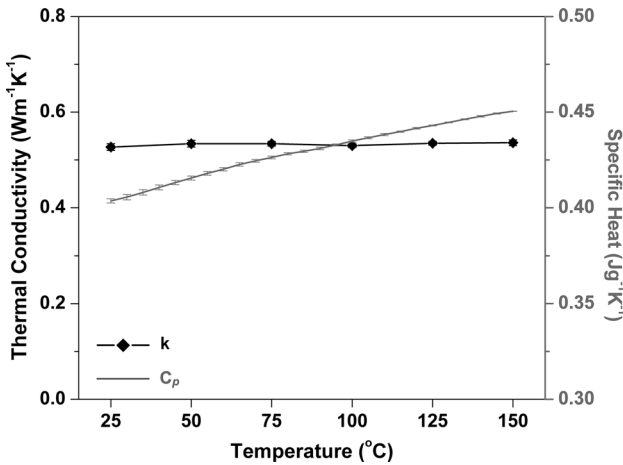
Fig. 5 XRD pattern of the as-sprayed GZO PSL

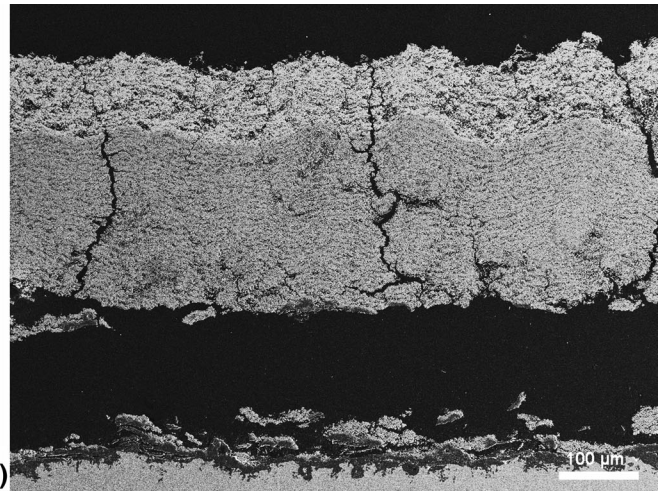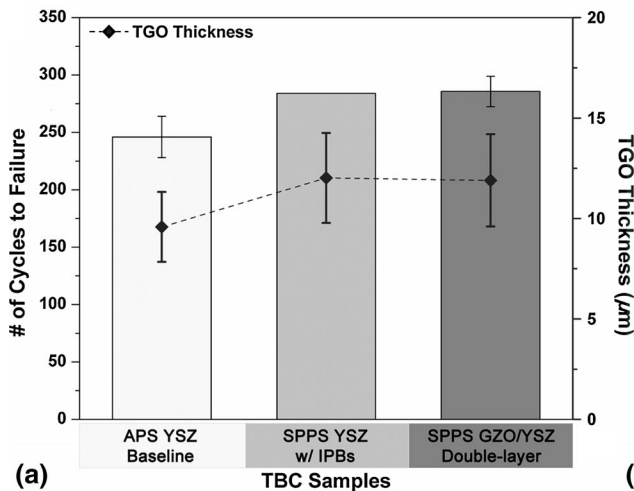**Fig. 6** Thermal conductivity and specific heat for the as-sprayed SPPS GZO PSL

fuel-rich (Ref 40) in this study, with GZO slightly close to the perfect stoichiometry. However, because of the heavy molecular weight of gadolinium, the GZO precursor with 50% gadolinium nitrate content has a lower *energy density* (heat per gram dried precursor gel), and thus reduced exothermic peaks (Table 4). In addition, a vigorous combustion reaction associated with high nitrate content is known to produce particles that are too fine to be deposited onto the substrates due to a smaller Stokes number (Ref 41) leading to many particles following the gas stream off the substrate instead of impacting it.

Surface tension (Table 4) can influence the droplet breakup mechanism during atomization, thus affecting the particle dimension and size distribution, heat transfer, entrainment, and overall microstructure of deposited coatings (Ref 41, 42). Given the higher surface tension of the GZO precursor, larger droplets were expected after air atomization, which would lead to enhanced droplets entrainment to the hot zone of plasma plume, full pyrolysis and melting of decomposed particles, and in return compensate for the disadvantages of using higher nitrate content. It was unclear though which of the competing dynamic and chemical factors would be dominant before actual spray trials.

3.2 Deposition and Characterization of the Double-Layer Coatings

The SPPS YSZ TBCs were optimized previously for prominent layered porosity and low thermal conductivity (Ref 29). The repeatability of microstructures based on specified processing parameters (Table 2) was proven viable in this current research, as microstructures containing thermal-conductivity-reducing IPBs were reproduced (Fig. 4c). Except for preheating the interlayers, no additional steps were needed for depositing the subsequent surface layers of GZO. Given the general similarity between GZO and YSZ in the precursor screening, especially in terms of dynamic viscosity and net heat
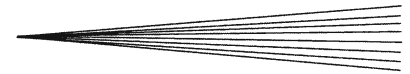

Fig. 7 (a) Summary of thermal cyclic durability and TGO thickness results based on a cyclic furnace test consisting of two OEM APS YSZ baseline, one SPPS YSZ with IPBs and four SPPS GZO/YSZ double-layer TBCs, and (b) failure mode of the SPPS double-layer TBC

(Table 4), processing parameters for GZO PSLs were derived from the parameters applied successfully for SPPS YSZ TBCs (Table 2); however, feed rate, stand-off distance, and cooling setup had to be adjusted to achieve the desired microstructure. By utilizing graphite planchets that can be burnt off above 600 °C, the calculation involving the weight and density of single-layer GZO revealed an approximate porosity of 15%, and in using this method all types of porosity were included. Vertical cracks (linear density: 180 μm^{-1}) were also observed in as-sprayed SPPS GZO PSLs as shown in Fig. 4.

From the SEM cross-sectional image (Fig. 4a), the adhesion between the SPPS GZO PSL and the YSZ inner layer appears to be good, with no apparent pores or gaps at the interface. Also important is the fact that desirable through-thickness vertical cracks extend from the YSZ interlayer to the GZO PSL, preserving the ability of the cracks to accommodate thermal expansion mismatch. The shared vertical cracks are able to accommodate the thermal expansion difference between YSZ and GZO (Ref 5), minimize the thermal stress accumulated under the thermal cyclic conditions, and therefore improve the durability of the double-layer TBCs, as is seen in Fig. 7.

Regarding the target thickness of each layer, Lee et al. not only mentioned that the double-layer GZO/YSZ structure could alleviate the overall compressive stress in TBCs, but also claimed the stress state was insensitive to the ratio of top-/bottom-layer thickness, unless the ratio was around 1:1 (Ref 43). Considering the economics and the erosion resistance of GZO (Ref 24), the thickness ratio of GZO:YSZ was kept at 1:2 for this research. However, it can be easily adjusted by altering the number of deposition passes for each layer.

Zirconates are known to form ordered pyrochlore or disordered fluorite structures at varying temperatures (Ref 8, 19); GZO is no exception, as the high-temperature stable fluorite phase tends to thermodynamically transform into pyrochlore with gradual cooling (Ref 44). However, a rapid-solidification process such as the solution spray (10^6 K s^{-1} or higher), together with the complicated physical and chemical reactions associated with the precursor pyrolysis, can lead to the preservation of metastable phases in the as-deposited coatings. Figure 5 shows the x-ray diffractogram of the as-sprayed SPPS GZO PSLs, in which the primary peaks suggest the predominant presence of the metastable fluorite phase, while the characteristic superlattice peaks of the pyrochlore phase, (311), (331), and (511), appear to be extremely weak. This suppressed formation of highly ordered pyrochlore phase in as-sprayed SPPS GZO is in accordance with the observations from both APS (Ref 17, 24) and EB-PVD (Ref 45) processes.

Thermal conductivity is another key property for TBC materials. Bulk YSZ has a thermal conductivity of 2.3 W m^{-1} K^{-1} at elevated temperatures, but this value can be reduced to 0.63 W m^{-1} K^{-1} through processing and microstructural engineering, e.g., the introduction of IPBs using the SPPS process (Ref 29). GZO (both pyrochlore and fluorite) has a lower bulk thermal conductivity of 1.6 W m^{-1} K^{-1} (Ref 19), and two consecutive mea-surements on two different as-sprayed SPPS GZO PSLs yielded an average thermal conductivity to be 0.55 W m^{-1} K^{-1} (Fig. 6). The lower thermal conductivity of both layers compared to APS YSZ ensured an overall low thermal conductivity in the double-layer TBC system.

3.3 Thermal Cyclic Durability Testing

The earlier tests dedicated to low-thermal-conductivity SPPS YSZ TBCs with IPBs demonstrated a promising durable performance (Ref 29). In this study, all three different TBC systems (APS YSZ supplied by OEM, SPPS YSZ with IPBs and SPPS GZO/YSZ double-layer) (Table 1) were tested side by side in 1-h cyclic furnace tests run at 1121 °C, and compared for thermal cyclic durability based on the cyclic lifetime and spallation mechanism.

By comparing the cyclic lives against the APS YSZ baseline samples, it is clear in Fig. 7a that SPPS TBCs exhibit improved durability, even though the relatively thicker SPPS TBCs would theoretically store more strain energy and have shorter cyclic lifetime. The average life-times of the SPPS TBCs (between SPPS YSZ with IPBs and SPPS GZO/YSZ double-layer), on the other hand, are comparable, indicating no notable deterioration of thermal cyclic durability is caused by the lower toughness of GZO PSLs (Ref 22).

Spallation was found to be at the YSZ/TGO interface in all cases (Fig. 7b), and durability was likely governed by the stresses in the ceramic associated with the TGO thickening. According to the measured TGO thickness at failure (Fig. 7a), SPPS coatings that had the stain-tolerant vertical cracks withstood somewhat thicker TGOs compared to APS OEM coatings. These stress-relieving vertical cracks also helped to stabilize the GZO/YSZ interface for the double-layer TBCs, which could be crack initiation sites due to the thermal expansion mismatch and the different sintering rates as seen in APS coatings of this same type (Ref 17), but as shown in the cross-sectional micrograph stayed almost intact without visible signs of crack initiation or propagation.

3.4 CMAS Resistance Tests

Spritz and paste tests were adopted for assessing the CMAS resistance of the single-layer APS as well as SPPS YSZ TBCs, and the double-layer YSZ/GZO TBC. Yet choosing the composition for testing remained an issue, providing CMAS is known to differ remarkably between locations, environments, and sources (Ref 20). Optical basicity has recently been proposed to be effective in predicting the reactivity between topcoat materials and CMAS, and of all simulated CMAS compositions reported in the literature, the optical basicity fell into a narrow range around 0.64, regardless of the different concentrations of individual constituent (Ref 46). This has led to the confident selection of the three simulated CMAS compositions, namely the 4-, 7-, and 9-component CMAS (Table 3), and the yielded CMAS-TBC interaction results were expected to be general to other compositions because of the similar optical basicity values.
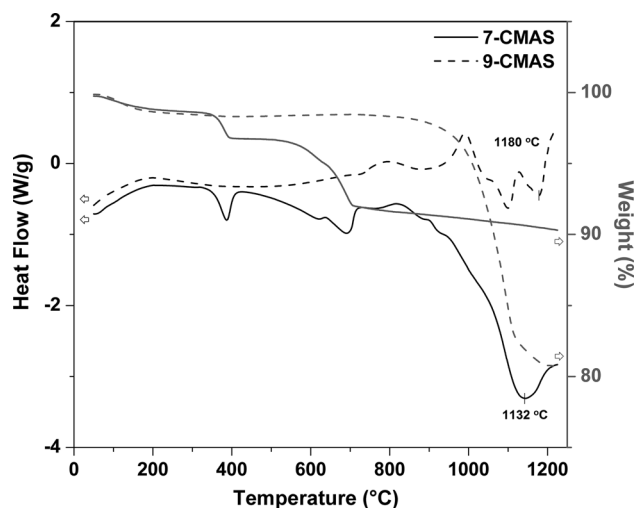
Fig. 8 Thermal characteristics of dried 7-/9-CMAS precursor gels

Fig. 9 Cyclic life of TBCs in CMAS spritz and paste tests

The initial melting point was the primary property of interest for all three simulated compositions: Drexler et al. showed the 4-CMAS to be molten at 1200 °C (Ref 21); but little published data were available for the 7- and 9-CMAS. After DSC-TGA measurements (Fig. 8), the melting point of 7-CMAS was found to be at 1132 °C, while for 9-CMAS, a value of 1180 °C was determined, even though some ingredients tended to complicate the measurement by decomposition. 4- and 9-CMAS were both utilized for spritz tests, as they would differentiate the effect of CMAS compositions if there was any, while the 7-CMAS, which resembled mostly to the 4-CMAS (Table 3), was selected specifically for the paste test, as the much lower melting point would ensure CMAS to attack the TBCs the same way as it would in actual engine environments at the determined testing temperature of 1180 °C. The heat-up duration in furnace cycles was also adjusted from 5 to 10 min, to accommodate the drastic testing conditions and avoid any potential furnace damage.

Cyclic life data of a limited number of TBC samples were gathered (Fig. 9) and used as one of the indicators of CMAS resistance in both spritz and paste tests. For most cases only one sample was tested for each condition, except for two double-layer TBCs spritzed with the 9-CMAS precursor. Although not statistically rigorous, the one and only replicated test was consistent with there being relatively modest scatter in these tests. Besides, OEM APS YSZ baselines (containing 10-15% porosity) were treated alongside with other SPPS TBCs for a direct comparison. Based on this limited testing, it is clear that periodically spraying CMAS precursors over coating surfaces did shorten the cyclic lifetime significantly, regardless of the CMAS composition due to the similar optical basicity; but if we look into the group of SPPS YSZ alone, spritzing deionized water (solvent) didn't affect the cyclic life much, as opposed to the case of no CMAS application (51 versus 55 cycles). This implies that the thermal shock of room-temperature water in contact of hot TBC surfaces was of
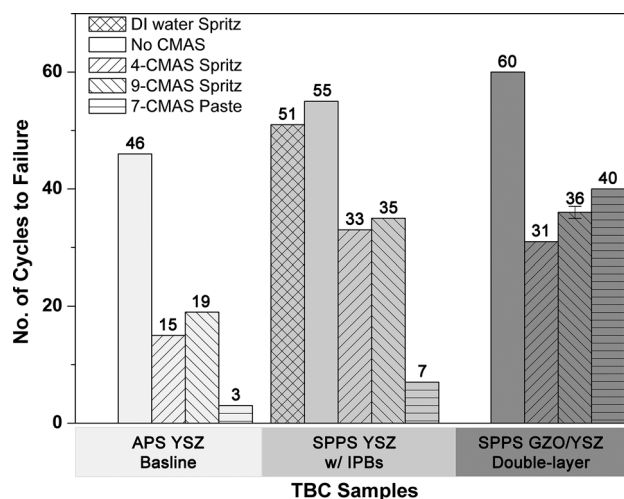
minimal effect to sample failures, and thereby the reduction in TBCs lives under spritz conditions was mostly due to CMAS attack. Secondly, when compared across all three TBC groups, Figure 9 indicates that SPPS TBCs, whether single- or double-layer, generally withstands more thermal cycles than APS TBCs do. This result, together with the thermal cycling test, suggests the strain-tolerant microstructure improves cyclic durability both with (Fig. 9) and without CMAS (Fig. 7). The stress-relieving vertical cracks alleviated the damage caused by the penetration of CMAS into the vertical cracks and small pores (Fig. 10a2). Between the single- and double-layer SPPS TBCs, little difference in cyclic lives was observed under spritz conditions. Contrary to an earlier study (Ref 18), the GZO layer in this study did not improve CMAS resistance. Given the fact that CMAS did attack the TBCs and shorten the cyclic lifetime, this contradictory phenomenon was unlikely to be the results of CMAS not being effective, but rather due to spritz conditions not being able to reproduce the CMAS infiltration-inhibiting reaction of GZO PSLs.

The paste test, with a one-time application of a greater amount of CMAS over coating surfaces followed by the same 1180 °C 1-h furnace cycles, was therefore employed to complement the assessment of CMAS resistance. The 7-CMAS was chosen in this case, since its low melting point would facilitate CMAS infiltration and prevent the cooling fan from blowing the paste away between cycles. As opposed to the spritz test, the double-layer SPPS GZO/YSZ TBCs this time lasted nearly six times longer than the SPPS YSZ TBCs and over 13 times longer than the APS YSZ baseline.

Another indicator of CMAS resistance was the assessment of cross-sectional images (Fig. 10). In spritz tests, spallation in all three TBC systems occurred close to the topcoat/TGO interfaces, again similar to the cyclic durability test. As mentioned earlier, CMAS attacks were observable; for in the case of SPPS YSZ with IPBs, the layered porosity gradually filled with molten glassy melt
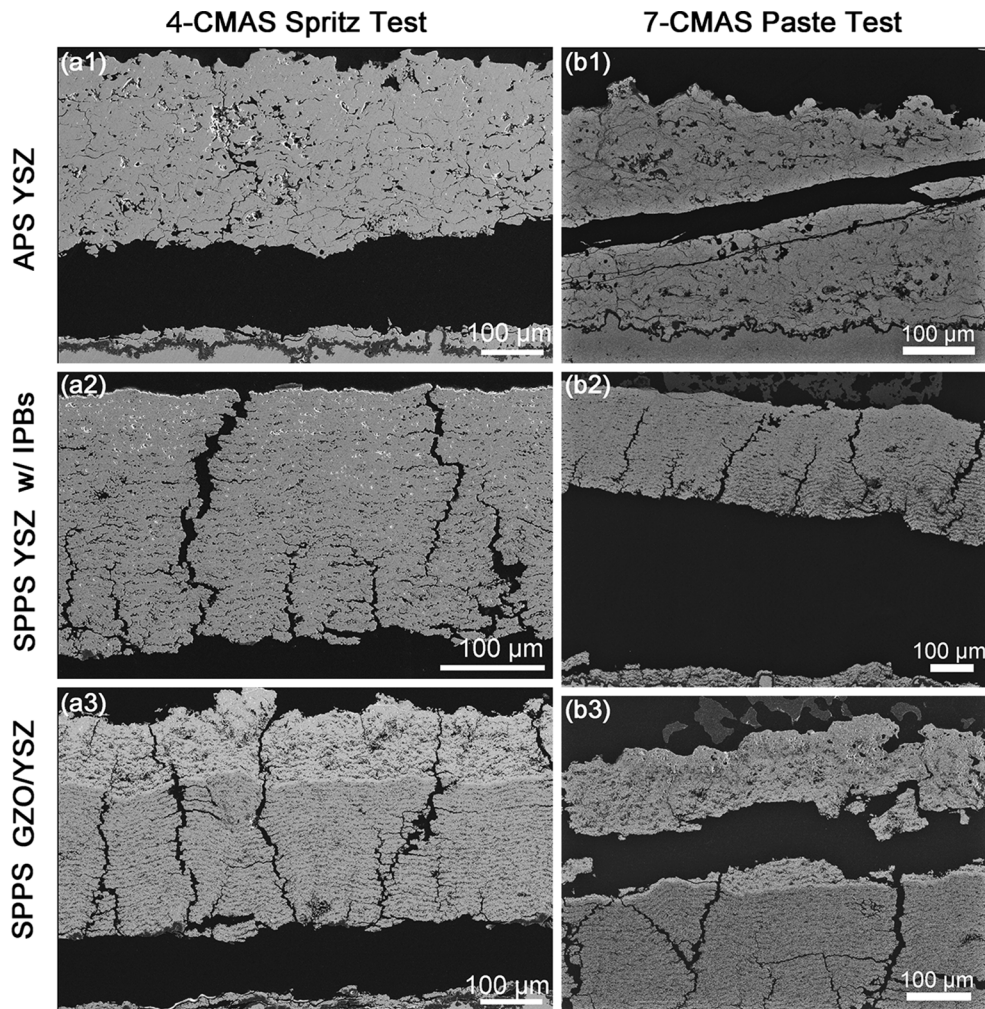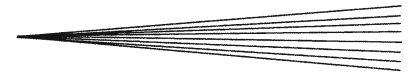
4-CMAS Spritz Test   **7-CMAS Paste Test**

APS YSZ

SPPS YSZ w/ IPBs

SPPS GZO/YSZ

Fig. 10 Comparison of failure sites between both CMAS resistance tests

(Fig. 10a2) as they got closer to the coating surface. While in the paste tests, each TBC system displayed a different failure mode (Fig. 10 b1/b2/b3): (1) for OEM APS YSZ, cracks were propagated from the topcoat surface to the TGO, leaving behind a flakey appearance, while segments above the spallation site were fully infiltrated with CMAS; (2) for SPPS YSZ with IPBs, coatings delamination occurred at TGO to topcoat interface, right beneath where CMAS fully penetrated the coating; and (3) for SPPS GZO/YSZ double-layer TBCs, the spallation was sporadically spotted close to the PSL/interlayer interface with CMAS trapped half-way in the GZO layer (Fig. 11b), while the underlying SPPS YSZ was protected and remained intact.

In summary, both the spritz and paste tests were used in this study to evaluate coatings' CMAS resistance under engine-relevant environments. The spritz test was preferred at first as it better simulates the periodic uptake of particle impurities in engines; however, the measured TBC lifetime to failure turned out to be primarily associated with the stress-relieving microstructure rather than the infiltration-inhibiting top layer. The paste tests, which

represent only a few scenarios, such as sandstorms or long-time CMAS built-up melting later under extreme operating conditions, succeeded in capturing the inhibition reaction and demonstrated the advantage of GZO PSLs. As shown in Fig. 11, the calcium distribution in the failed double-layer SPPS GZO/YSZ TBCs were characterized with SEM/EDS either just above the topcoat/TGO interface for the spritz test, or around the GZO/YSZ interface for the paste test. It was then demonstrated that in the spritz test the protective mechanisms known for GZO were not effective in protecting the TBC from CMAS infiltration, whereas they were effective in the paste test.

The drastic difference between these two tests raises a question: what leads to the protective mechanism in the GZO. The amount of CMAS and how the CMAS are applied are likely answers. The formation kinetics of blocking phases and CMAS infiltration rates are competing, inter-related factors in terms of CMAS attack. When CMAS was repeatedly applied at a small dose in an isothermal environment (spritz tests), infiltration outweighed the formation of blocking phase (Fig. 11a),
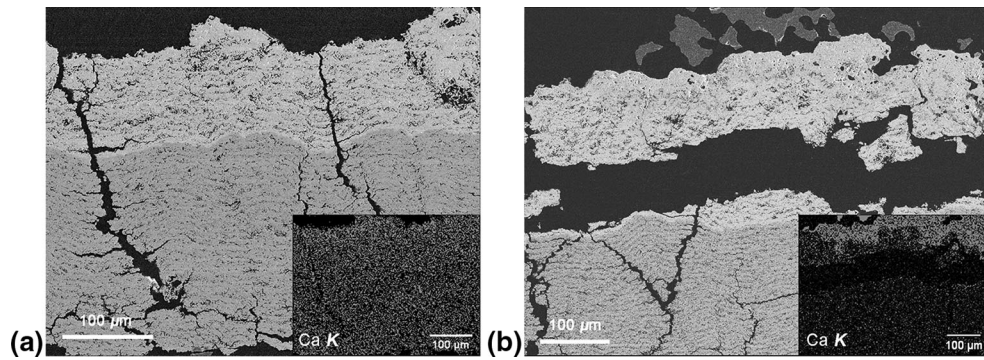
Fig. 11 SEM/EDS cross-sectional images of SPPS GZO/YSZ double-layer samples showing (a) CMAS infiltrated through both TBC layers in the spritz test while (b) CMAS trapped in the GZO PSL under paste conditions
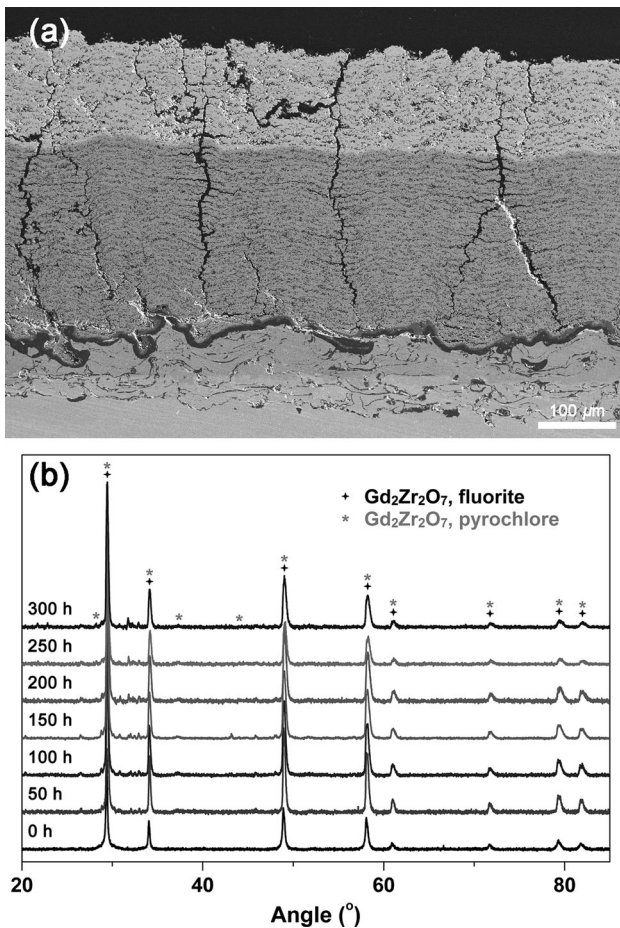

Fig. 12 High temperature steam test after 300 h: (a) cross-section micrograph showing interface stability in the SPPS double-layer microstructure, and (b) overlaid GZO PSL XRD patterns showing the phase stability

leading to continuing CMAS attack. Due to the small doses, the damage was progressive; therefore, the test itself resembled the thermal cyclic durability test with possible additional effects from the growing stresses on the TGO surface. While in the paste test, the formation kinetics of blocking phases was accelerated by the exces-sive amount of CMAS paste in the first cycle, and initiated the protective mechanism of GZO (Fig. 11b), preventing CMAS from further attacking the TBC. In the end, the characterization of CMAS resistance is intricate and lar-gely dependent on the testing conditions, which are deemed "representative" of engine environments.

3.5 High Temperature Steam Tests

High temperature steam was another concern for alternative TBC systems to be used at elevated tempera-tures, such as in IGCC environments. After 300 h of heat treatment in the test rig (Fig. 2), SEM micrographs showed clear and intact interfaces at PSL/interlayer and topcoat/TGO, with the strain-tolerant vertical cracks that run through both layers unchanged (Fig. 12a). No change in the diffraction pattern was evident during heat treat-ment (Fig. 12b) including the preservation of the pre-dominant fluorite phase, which suggested the phases in the GZO PSLs were stable in the high-temperature humid environments. In parallel tests, APS and SPPS YSZ TBCs alone also retained the t'-phase under the same moist conditions. As for the interfacial regions between GZO/YSZ, SEM secondary/backscattered signals revealed no observable changes. A smaller size scale interface char-acterization may be needed using TEM imaging, but in this limited testing, the double-layer TBCs, consisting of SPPS GZO PSLs and YSZ interlayers, showed no signs of formation of new phases under high temperature steam.

4. Conclusions

The SPPS process was successfully employed in this study to deposit a double-layer TBC topcoat, consisting of a CMAS infiltration-inhibiting gadolinium zirconate pro-tective surface layer and an SPPS-deposited YSZ layer with a thermal conductivity that is roughly half of that of a typical APS TBC. The lower conductivity in the YSZ interlayer was achieved by having layered porosity re-ferred to as IPBs. The deposited GZO PSLs have a mix of low-thermal-conductivity pyrochlore and fluorite phases, and strain-tolerant, vertically cracked microstructures,
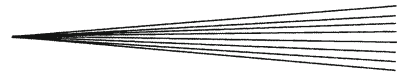
which are inherent to the SPPS process. The thermal cyclic durability of double-layer SPPS GZO/YSZ TBCs was shown to be comparable to single-layer SPPS YSZ TBCs and superior to the APS YSZ baseline. Unlike previous APS double-layer coatings (Ref 17), no failures were observed at the GZO to YSZ interface.

To validate the improvement of CMAS resistance in the double-layer SPPS GZO/YSZ TBCs, a thermal gradient test would be ideal; however, limited by equipment availability, two isothermal-furnace-based cyclic tests were used instead, namely the CMAS spritz and paste tests. Both tests showed the SPPS TBCs outlived APS YSZ baselines, indicating better resistance. Furthermore, the GZO PSLs were directly shown in SEM/EDS to arrest CMAS penetration front, and thereby protect the underlying materials and extend the TBC's cyclic life by sixfold in the paste tests. In contrast, the spritz tests failed to distinguish the two SPPS TBC systems, showing no obvious benefit to CMAS resistance with the addition of GZO PSLs, which raises the question what qualifies realistic testing conditions in terms of CMAS application. To evaluate TBCs' performance under IGCC environments, the double-layer SPPS GZO/YSZ TBCs was also tested under high-temperature steam using an in-house-built steam rig, and exhibited favorable phase and microstructural stability up to 300 h.

Acknowledgments

References

1. N.P. Padture, M. Gell, and E.H. Jordan, Thermal Barrier Coatings for Gas-Turbine Engine Applications, *Science*, 2002, **296**(5566), p 280-284
2. A.G. Evans, D.R. Mumm, J.W. Hutchinson, G.H. Meier, and F.S. Pettit, Mechanisms Controlling the Durability of Thermal Barrier Coatings, *Prog. Mater. Sci.*, 2001, **46**(5), p 505-553
3. D.R. Clarke, M. Oechsner, and N.P. Padture, Thermal Barrier Coatings for More Efficient Gas-Turbine Engines, *MRS Bull.*, 2012, **37**(10), p 891-898
4. J.H. Perepezko, The Hotter the Engine, the Better, *Science*, 2009, **326**(5956), p 1068-1069
5. R. Vassen, A. Stuke, and D. Stöver, Recent Developments in the Field of Thermal Barrier Coatings, *J. Therm. Spray Technol.*, 2009, **18**(2), p 181-186
6. M.P. Borom, C.A. Johnson, and L.A. Peluso, Role of Environmental Deposits and Operating Surface Temperatures in Spallation of Air Plasma Sprayed Thermal Barrier Coatings, *Surf. Coat. Technol.*, 1996, **86--87**, p 116-126
7. L. Li, N. Hitchman, and J. Knapp, Failure of Thermal Barrier Coatings Subjected to CMAS Attack, *J. Therm. Spray Technol.*, 2010, **19**(1–2), p 148-155
8. D.R. Clarke and S.R. Phillpot, Thermal Barrier Coating Materials, *Mater. Today*, 2005, **8**(6), p 22-29
9. G. Mauer, M.O. Jarligo, D.E. Mack, and R. Vassen, Plasma-Sprayed Thermal Barrier Coatings: New Materials, Processing Issues, and Solutions, *J. Therm. Spray Technol.*, 2013, **22**(5), p 646-658
10. M.J. Maloney, Thermal Barrier Coating Systems and Materials. US Patent 6177200, 2001
11. R. Vassen, X. Cao, F. Tietz, B. Basu, and D. Stöver, Zirconates as New Materials for Thermal Barrier Coatings, *J. Am. Ceram. Soc.*, 2000, **83**(8), p 2023-2028
12. W. Ma, D. Mack, J. Malzbender, R. Vassen, and D. Stöver, Yb_2O_3 and Gd_2O_3 Doped Strontium Zirconate for Thermal Barrier Coatings, *J. Eur. Ceram. Soc.*, 2008, **28**(16), p 3071-3081
13. M.O. Jarligo, G. Mauer, D. Sebold, D.E. Mack, R. Vassen, and D. Stöver, Decomposition of $Ba(Mg_{1/3}Ta_{2/3})O_3$ Perovskite During Atmospheric Plasma Spraying, *Surf. Coat. Technol.*, 2012, **206**(8–9), p 2515-2520
14. Y.J. Su, R.W. Trice, K.T. Faber, H. Wang, and W.D. Porter, Thermal Conductivity, Phase Stability, and Oxidation Resistance of $Y_3Al_5O_{12}$ (YAG)/Y_2O_3-ZrO_2 (YSZ) Thermal-Barrier Coatings, *Oxid. Met.*, 2004, **61**(3), p 253-271
15. E.H. Jordan, M. Gell, C. Jiang, J. Wang, and B. Nair, High Temperature Thermal Barrier Coating Made by the Solution Precursor Plasma Spray Process, *ASME Turbo Expo 2014: Turbine Technical Conference and Exposition*, Dusseldorf, Germany, 2014
16. N.P. Bansal and D. Zhu, Thermal Properties of Oxides with Magnetoplumbite Structure for Advanced Thermal Barrier Coatings, *Surf. Coat. Technol.*, 2008, **202**(12), p 2698-2703
17. E. Bakan, D.E. Mack, G. Mauer, and R. Vassen, Gadolinium Zirconate/YSZ Thermal Barrier Coatings: Plasma Spraying, Microstructure, and Thermal Cycling Behavior, *J. Am. Ceram. Soc.*, 2014, **97**(12), p 4045-4051
18. S. Kraemer, J. Yang, and C.G. Levi, Infiltration-Inhibiting Reaction of Gadolinium Zirconate Thermal Barrier Coatings with CMAS Melts, *J. Am. Ceram. Soc.*, 2008, **91**(2), p 576-583
19. J. Wu, X. Wei, N.P. Padture, P.G. Klemens, M. Gell, E. Garcia, P. Miranzo, and M.I. Osendi, Low-Thermal-Conductivity Rare-Earth Zirconates for Potential Thermal-Barrier-Coating Applications, *J. Am. Ceram. Soc.*, 2002, **85**(12), p 3031-3035
20. C.G. Levi, J.W. Hutchinson, M.-H. Vidal-Setif, and C.A. Johnson, Environmental Degradation of Thermal-Barrier Coatings by Molten Deposits, *MRS Bull.*, 2012, **37**(10), p 932-942
21. J.M. Drexler, A.L. Ortiz, and N.P. Padture, Composition Effects of Thermal Barrier Coating Ceramics on their Interaction with molten Ca-Mg-Al-Silicate (CMAS) Glass, *Acta Mater.*, 2012, **60**(15), p 5437-5447
22. U. Bast and E. Schumann, Development of Novel Oxide Materials for TBCs, *Ceram. Eng. Sci. Proc.*, 2002, **23**(4), p 525-532
23. R. Vassen, F. Treager, and D. Stöver, New Thermal Barrier Coatings Based on Pyrochlore/YSZ Double-Layer Systems, *Int. J. Appl. Ceram. Technol.*, 2004, **1**(4), p 351-361
24. G. Dwivedi, Y. Tan, V. Viswanathan, and S. Sampath, Process-Property Relationship for Air Plasma-Sprayed Gadolinium Zirconate Coatings, *J. Therm. Spray Technol.*, 2015, **24**(3), p 454-466
25. R.M. Leckie, S. Kraemer, M. Ruhle, and C.G. Levi, Thermochemical Compatibility Between Alumina and ZrO_2-$GdO_{3/2}$ Thermal Barrier Coatings, *Acta Mater.*, 2005, **53**(11), p 3281-3292
26. D.R. Clarke and C.G. Levi, Materials Design for the Next Generation Thermal Barrier Coatings, *Annu. Rev. Mater. Res.*, 2003, **33**(1), p 383-417
27. M. Gell, E.H. Jordan, M. Telcholz, B.M. Cetegen, N.P. Padture, L. Xie, D. Chen, X. Ma, and J. Roth, Thermal Barrier Coatings Made by the Solution Precursor Plasma Spray Process, *J. Therm. Spray Technol.*, 2008, **17**(1), p 124-135
28. A.D. Jadhav and N.P. Padture, Mechanical Properties of Solution-Precursor Plasma-Sprayed Thermal Barrier Coatings, *Surf. Coat. Technol.*, 2008, **202**(20), p 4976-4979
29. E.H. Jordan, C. Jiang, J. Roth, and M. Gell, Low Thermal Conductivity Yttria-Stabilized Zirconia Thermal Barrier Coatings Using the Solution Precursor Plasma Spray Process, *J. Therm. Spray Technol.*, 2014, **23**(5), p 849-859
30. A.D. Jadhav, N.P. Padture, F. Wu, E.H. Jordan, and M. Gell, Thick Ceramic Thermal Barrier Coatings with High Durability

Deposited Using Solution-Precursor Plasma Spray, *Mater. Sci. Eng. A*, 2005, **405**(1–2), p 313-320

31. D. Chen, E.H. Jordan, M. Gell, and X. Ma, Dense TiO₂ Coating Using the Solution Precursor Plasma Spray Process, *J. Am. Ceram. Soc.*, 2008, **91**(3), p 865-872

32. D. Chen, E.H. Jordan, M.W. Renfro, and M. Gell, Dy:YAG Phosphor Coating Using the Solution Precursor Plasma Spray Process, *J. Am. Ceram. Soc.*, 2009, **92**(1), p 268-271

33. C.K. Muoto, E.H. Jordan, M. Gell, and M. Aindow, Identification of Desirable Precursor Properties for Solution Precursor Plasma Spray, *J. Therm. Spray Technol.*, 2011, **20**(4), p 802-816

34. F. Wu, E.H. Jordan, X. Ma, and M. Gell, Thermally Grown Oxide Growth Behavior and Spallation Lives of Solution Precursor Plasma Spray Thermal Barrier Coatings, *Surf. Coat. Technol.*, 2008, **202**(9), p 1628-1635

35. J.R. Davis, Environmental stability: bond coat stability, *Handbook of Thermal Spray Technology*, ASM International, Materials Park, 2004, p 270

36. A. Bolcavage, A. Feuerstein, J. Foster, and P. Moore, Thermal Shock Testing of Thermal Barrier Coating/Bondcoat Systems, *J. Mater. Eng. Perform.*, 2004, **13**(4), p 389-397

37. T. Steinke, D. Sebold, D.E. Mack, R. Vassen, and D. Stöver, A Novel Test Approach for Plasma-Sprayed Coatings Tested Simultaneously Under CMAS and Thermal Gradient Cycling Conditions, *Surf. Coat. Technol.*, 2010, **205**(7), p 2287-2295

38. R. Wellman, G. Whitman, and J.R. Nicholls, CMAS Corrosion of EB-PVD TBCs: Identifying the Minimum Level to Initiate Damage, *Int. J. Refract. Met. Hard Mater.*, 2010, **28**(1), p 124-132

39. W. Zhao and B. Gleeson, Steam Effects on the Oxidation Behavior of Al₂O₃-Scale Forming Ni-Based Alloys, *Oxid. Met.*, 2013, **79**(5), p 613-625

40. S.R. Jain, K.C. Adiga, and V.R. PaiVerneker, A New Approach to Thermochemical Calculations of Condensed Fuel-Oxidizer Mixtures, *Combust. Flame*, 1981, **40**, p 71-79

41. P. Fauchais, R. Etchart-Salas, V. Rat, J.F. Coudert, N. Caron, and K. Wittmann-Teneze, Parameters Controlling Liquid Plasma Spraying: Solutions, Sols, or Suspensions, *J. Therm. Spray Technol.*, 2008, **17**(1), p 31-59

42. R. Rampon, O. Marchand, C. Filiatre, and G. Bertrand, Influence of Suspension Characteristics on Coatings Microstructure Obtained by Suspension Plasma Spraying, *Surf. Coat. Technol.*, 2008, **202**(18), p 4337-4342

43. D. Lee, T.W. Kim, and K.S. Lee, Design of Thermal Barrier Coatings Using Gadolinium Zirconate Ceramis: A Study on Gadolinium Zirconate/YSZ Bilayers, *J. Ceram. Soc. Jpn.*, 2009, **117**(5), p 550-554

44. S. Lakiza, O. Fabrichnaya, C. Wang, M. Zinkevich, and F. Aldringer, Phase Diagram of the ZrO₂-Gd₂O₃-Al₂O₃ System, *J. Eur. Ceram. Soc.*, 2006, **26**(3), p 233-246

45. A.U. Munawar, U. Schulz, G. Cerri, and H. Lau, Microstructure and Cyclic Lifetime of Gd and Dy-Containing EB-PVD TBCs Deposited as Single and Double-Layer on Various Bond Coats, *Surf. Coat. Technol.*, 2014, **245**, p 92-101

46. A.R. Krause, B.S. Senturk, H.F. Garces, G. Dwivedi, A.L. Ortiz, S. Sampath, and N.P. Padture, 2ZrO₂:Y₂O₃ Thermal Barrier Coatings Resistant to Degradation by Molten CMAS: Part I, Optical Basicity Considerations and Processing, *J. Am. Ceram. Soc.*, 2014, **97**(12), p 3943-3949